

Transfer functions of a transformer at different values of coupling coefficient

ISSN 1751-858X

Received on 29th April 2015

Revised on 14th December 2015

Accepted on 17th December 2015

doi: 10.1049/iet-cds.2015.0147

www.ietdl.org

Agasthya Ayachit , Marian Kazimierz Kazimierczuk

Department of Electrical Engineering, Wright State University, Dayton, OH 45435, USA

 E-mail: ayachit.2@wright.edu

Abstract: The low- and mid-frequency model of the transformer with resistive load is analysed for different values of coupling coefficients. The model comprising of coupling-dependent inductances is used to derive the following characteristics: voltage gain, current gain, bandwidth, input impedance, and transformer efficiency. It is shown that in the low- and mid-frequency range, the turns ratio between the windings is a strong function of the coupling coefficient, i.e., if the coupling coefficient decreases, then the effective turns ratio reduces. A practical transformer was designed, simulated, and tested. It was observed that the magnitudes of the voltage transfer function and current transfer function exhibit a maximum value each at a different value of coupling coefficient. In addition, as the coupling coefficient decreases, the transformer bandwidth also decreases. Furthermore, analytical expressions for the transformer efficiency for resistive loads are derived and its variation with respect to frequency at different coupling coefficients is investigated. It is shown that the transformer efficiency is maximum at any coupling coefficient if the input resistance is equal to the load resistance. Experimental validation of the theoretical results was performed using a practical transformer set-up. The theoretical predictions were found to be in good agreement with the experimental results.

1 Introduction

Transformers are an integral part of many circuits used in various applications [1–41]. The transformer constitutes the magnetic core and the windings, whose linear or non-linear physical attributes such as core resistance, winding resistance, leakage fluxes etc., are frequency and temperature dependent [1–4]. As the transformers are designed to operate at frequencies ranging from almost dc to several megahertz, these physical attributes show dominance at different ranges of frequencies. Also, the components such as leakage inductances and the magnetising inductance show strong dependence on the strength of the magnetic coupling between the windings. Analysis of the effect of coupling coefficient on these physical attributes is of great practical importance.

The behavioural model of the transformer is categorised as the low-frequency model and the high-frequency model [5–20]. The low-frequency model comprises of the magnetising inductance, leakage inductances, and the dc resistances of the primary and secondary windings. On the other hand, the high-frequency model takes into account the parasitic capacitance of the transformer windings, frequency-dependent permeability of the magnetic core, and the frequency-dependent winding resistances. Achieving a complete and an exact model of the transformer, which represents all the low- and high-frequency effects is a challenge.

This paper derives the transfer functions pertaining to the low- and mid-frequency models of the non-ideal transformer. The analysis also forms a basis for understanding the high-frequency model of the transformer. In this paper, frequencies from 10 Hz to 100 kHz typically lie in the low- and mid-frequency regions, whereas frequencies beyond 100 kHz usually are in the high-frequency region.

The objectives of this paper are as follows:

- (i) to adopt the low- and mid-frequency model of the transformer that includes the magnetising inductance, leakage inductances, and dc winding resistances;
- (ii) to derive the expressions for voltage transfer function, current transfer function, input impedance, bandwidth (BW), and transformer efficiency;

- (iii) to analyse the transformer characteristics as functions of frequency at different values of coupling coefficient;
- (iv) to determine the maximum magnitudes of the voltage gain and current gain and the BW of the transformer; and
- (v) to determine the useful range of frequencies in which the maximum power transfer takes place.

This paper is categorised as follows: Section 2 describes the low- and mid-frequency models of the transformer that is considered in this analysis. Section 3 presents the derivation of the transfer functions such as the input impedance, voltage gain, and current gain of the transformers in the frequency domain. Section 4 derives the expression for the efficiency of the transformer with resistive loads. A practical transformer design is performed, the presented theory is analysed, and experimental results are presented in Section 5. Finally, Section 6 provides the conclusions and suggests future work.

2 Equivalent model

2.1 Assumptions

The following assumptions are made in this paper, which are applicable for the low- and mid-frequency analyses of the transformers:

- The core resistance due to the core losses, which is in parallel to the magnetising inductance is neglected in this analysis. It was observed by the authors that the core resistance did not alter the low-frequency characteristics, but increased the complexity in the derivation of the gain and impedance expressions.
- The imaginary part of the complex permeability is negligible at low frequencies. Therefore, only the real part of the complex permeability is considered and the value of the effective permeability is constant in the low- to mid-frequency range. The validity of this assumption is discussed in Section 5.
- The effects due to fringing flux are neglected.

- The winding resistances are frequency and temperature independent.
- The parasitic capacitances of the transformer windings are negligible.
- The transformer is loaded by a linear resistance.

2.2 Low- and mid-frequency equivalent models

Fig. 1a shows the circuit of a two-winding transformer, where L_p and L_s represent the self-inductances of the primary and secondary windings, respectively. Each winding is wound on one separate part of the magnetic core. The coupling coefficient k is varied by changing the distance between the windings. Fig. 1b shows the low- and mid-frequency model of the transformer depicted in Fig. 1a [1]. The components r_p and r_s represent the winding dc resistance of the primary and secondary windings, respectively. The inductances L_{lp} and L_{ls} represent the leakage inductance of the primary and secondary windings, respectively. The magnetising inductance is considered on the primary.

The turns ratio of an ideal transformer is given by

$$n = \frac{N_p}{N_s}, \quad (1)$$

where N_p is the number of turns of the primary winding and N_s is the number of turns of the secondary winding. Both halves of the core are identical such that the area of the core cross-section is equal and the mean magnetic path length of the primary and secondary windings is also equal. Therefore, the mutual coupling between the primary to secondary windings and *vice versa* are equal. The mutual inductance between the primary and secondary is given by

$$M = k\sqrt{L_p L_s}, \quad (2)$$

where k represents the coupling coefficient between the primary and secondary windings or *vice versa*. The coupling coefficient depends on the distance of separation between the two windings. The self-inductance of the primary winding is given as

$$L_p = \frac{\mu A_c N_p^2}{l_c}, \quad (3)$$

where A_c represents the cross-sectional area of the common flux in the cores, l_c is the mean path length of the magnetic flux linking the primary and secondary windings, and $\mu = \mu_0 \mu_r$ is the permeability of the cores. Similarly, the self-inductance of the

secondary winding is given by

$$L_s = \frac{\mu A_c N_s^2}{l_c}. \quad (4)$$

From Fig. 1b, it can be stated that the inductances L_p and L_s constitute the ideal transformer and provides the required turns ratio, whereas the magnetic energy is stored within the magnetising inductance and both leakage inductances. The turns ratio and the self-inductance of perfectly coupled windings ($k=1$) are related as

$$n = \sqrt{\frac{L_p}{L_s}}. \quad (5)$$

The magnetising inductance is expressed as

$$L_m = kL_p = \frac{k\mu A_c N_p^2}{l_c}. \quad (6)$$

In transformers with loosely coupled windings, the leakage flux is significant and depends on the coupling between the two windings and is modelled as leakage inductances. The leakage inductance on the primary side is

$$L_{lp} = (1-k)L_p = \frac{(1-k)}{k}L_m. \quad (7)$$

Similarly, the leakage inductance on the secondary side is

$$L_{ls} = (1-k)L_s = \frac{(1-k)L_p}{n^2} = \frac{(1-k)}{n^2 k}L_m, \quad (8)$$

where $L_s = L_p/n^2$ and the inductance ratio is given in (5).

3 Input impedance, voltage gain, and current gain

In this section, the characteristics of the transformers such as input impedance, voltage gain, and current gain of the non-ideal transformer are analysed in the frequency domain. From Fig. 1b, the components in the transformer can be lumped and expressed as impedances given as follows

$$Z_p = r_p + j\omega L_{lp} = r_p + j\omega(1-k)L_p, \quad (9)$$

$$Z_m = j\omega L_m = j\omega kL_p, \quad (10)$$

$$Z_s = r_s + j\omega L_{ls} = r_s + j\omega(1-k)L_s. \quad (11)$$

The load impedance can be purely resistive, purely reactive, or a combination of resistance and reactance depending on the type of application. The load impedance is expressed as

$$Z_L = R_L + jX, \quad (12)$$

where R_L represents the load resistance and X represents the load reactance. The reactance X has a positive sign for inductive load and a negative sign for capacitive load. In this paper, resistive loads are considered ($Z_L = R_L$); however, the analysis can be extended to reactive loads also.

3.1 Input impedance

Fig. 2a shows the equivalent model of the transformer with the components on the secondary reflected to the primary. By

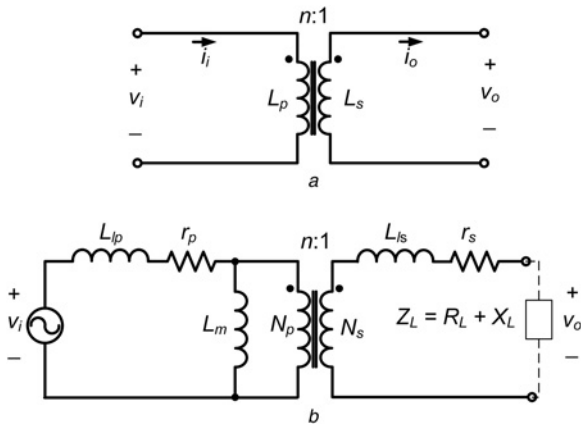


Fig. 1 Circuit and model of a two-winding transformer

a Circuit

b Low-frequency and mid-frequency model

inspection, the input impedance is

$$Z_i = Z_p + \frac{n^2 Z_m (Z_s + Z_L)}{Z_m + n^2 (Z_s + Z_L)}. \quad (13)$$

Substituting (9)–(12) into (13) yields for $Z_L = R_L$

$$Z_i = r_p + sL_{lp} + \frac{sL_m n^2 (sL_{ls} + r_s + R_L)}{sL_m + n^2 (sL_{ls} + r_s + R_L)}. \quad (14)$$

Modifying (14) results in

$$Z_i = r_p + sL_{lp} + \left(\frac{n^2 L_{ls} L_m}{n^2 L_{ls} + L_m} \right) \frac{S[s + [(r_s + R_L)/L_{ls}]]}{s + [n^2 (r_s + R_L)/(n^2 L_{ls} + L_m)]}. \quad (15)$$

The inductances in (15) can be expressed in terms of L_p , k , and n to obtain the expression for the input impedance in general form as

$$Z_i = r_p + s(1 - k)L_p + Z_x \frac{s(s + \omega_z)}{s + \omega_p}, \quad (16)$$

where

$$Z_x = \frac{n^2 L_{ls} L_m}{n^2 L_{ls} + L_m} = k(1 - k)L_p, \quad (17)$$

$$\omega_z = \frac{\omega_L}{1 - k} = \frac{(r_s + R_L)}{L_{ls}} = \frac{n^2 (r_s + R_L)}{(1 - k)L_p}, \quad (18)$$

and

$$\omega_p = \omega_L = \frac{n^2 (r_s + R_L)}{n^2 L_{ls} + L_m} = \frac{n^2 (r_s + R_L)}{L_p}. \quad (19)$$

Furthermore, the input impedance in the complex form is

$$Z_i = \mathcal{R}e\{Z_i\} + j\mathcal{I}m\{Z_i\} = R_i + jX_i, \quad (20)$$

where R_i is the input resistance and X_i is the input reactance. The

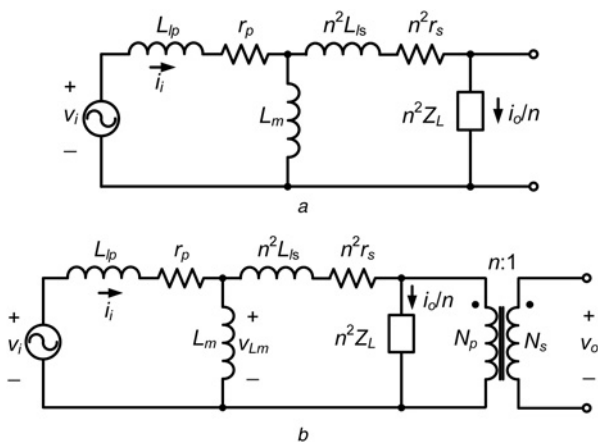


Fig. 2 Equivalent circuits to determine the input impedance, current gain, and voltage gain

a Model of the transformer to determine the input impedance Z_i and the current gain A_i
b Model of the transformer to determine the voltage gain A_v

magnitude of the input impedance is

$$|Z_i| = \sqrt{R_i^2 + X_i^2}, \quad (21)$$

and the phase of the input impedance is

$$\phi_{Z_i} = \tan^{-1} \left(\frac{X_i}{R_i} \right). \quad (22)$$

The real and imaginary components of the input impedance can be extracted by substituting $s = j\omega$ into (16). Thus, the input resistance R_i is

$$R_i = r_p - \frac{Z_x (\omega_p - \omega_z)}{1 + (\omega_p/\omega)^2}. \quad (23)$$

The extremities of the input resistance R_i can be determined as follows. At dc, $\omega = 0$ such that $\omega_p/\omega = \infty$ resulting in

$$R_i = r_p. \quad (24)$$

At mid- and high-frequencies, as $\omega \rightarrow \infty$, the term $\omega_p/\omega = 0$ leading to

$$R_i = r_p - Z_x (\omega_p - \omega_z) = r_p + (kn)^2 (r_s + R_L), \quad (25)$$

indicating that the transformer input resistance at mid-frequencies is a function of not only the turns ratio n , but also the coupling coefficient k . As the coupling coefficient reduces, the input resistance also reduces.

The input reactance is

$$\begin{aligned} X_i &= \omega L_{lp} + Z_x \frac{\omega^3 + \omega \omega_p \omega_z}{\omega^2 + \omega_p^2} \\ &= \omega(1 - k)L_p + Z_x \omega \frac{1 + (\omega_p \omega_z / \omega^2)}{1 + (\omega_p/\omega)^2}. \end{aligned} \quad (26)$$

The input inductance at any k is

$$\begin{aligned} L_i &= \frac{X_i}{\omega} = L_p(1 - k) + k(1 - k)L_p \frac{1 + \{\omega_p^2 / [(1 - k)\omega^2]\}}{1 + (\omega_p/\omega)^2} \\ &= L_p \left[(1 - k) + k \frac{1 - k + (\omega_p/\omega)^2}{1 + (\omega_p/\omega)^2} \right]. \end{aligned} \quad (27)$$

The input reactance at $k = 1$ is a special case, since the extremities of the input reactance are different from those obtained for $k < 1$. Substituting (17)–(19) into (26) and equating k to unity, we obtain

$$X_i = \frac{L_p \omega \omega_p^2}{\omega^2 + \omega_p^2} = \frac{\omega L_p}{1 + (\omega/\omega_p)^2}. \quad (28)$$

Thus, the input inductance at $k = 1$ is

$$L_i = \frac{X_i}{\omega} = \frac{L_p}{1 + (\omega/\omega_p)^2}. \quad (29)$$

At dc, $\omega = 0$, and X_i in (28) is also equal to zero. As $\omega \rightarrow \infty$, the input reactance $X_i \rightarrow \infty$. However, by inspection, X_i approaches a finite value, when $\omega \simeq \omega_p$ in the mid-frequency region. For any other value of $k < 1$, the value of the input reactance can be found

from (26), where at dc, $X_i=0$ as $\omega = 0$. As $\omega \rightarrow \infty$, then X_i also approaches infinity. The results of this theory are demonstrated in Section 5.

3.2 Current gain

The equivalent model shown in Fig. 2a can be used to estimate the current gain of the transformer. By inspection, the current gain is given by

$$A_i = \frac{i_o}{i_i} = \frac{nZ_m}{Z_m + n^2(Z_s + Z_L)}. \quad (30)$$

Substituting (10) and (11) into (30), the current gain in s -domain can be expressed as

$$\begin{aligned} A_i &= \frac{nsL_m}{sL_m + n^2[r_s + s(1-k)L_s + R_L]} \\ &= \frac{knsL_p}{s[kL_p + (1-k)L_p] + n^2(r_s + R_L)}, \end{aligned} \quad (31)$$

and in terms of L_p , we get

$$A_i = kn \frac{s}{s + \left[\frac{n^2(r_s + R_L)}{L_p} \right]} = A_{ix} \frac{s}{s + \omega_L}, \quad (32)$$

where A_{ix} is the mid- and high-frequency gain given by

$$A_{ix} = kn, \quad (33)$$

and the lower-cut-off frequency is

$$\omega_L = \frac{n^2(r_s + R_L)}{L_p}. \quad (34)$$

Equation (32) represents the transfer function of a first-order high-pass filter with a lower-cut-off frequency ω_L and a gain A_{ix} . Substituting $s = j\omega$ into (32), we obtain

$$A_i = A_{ix} \frac{j\omega}{j\omega + \omega_L} = \frac{A_{ix}}{1 - j(\omega_L/\omega)}. \quad (35)$$

Using $\omega = 2\pi f$, the magnitude of the current gain can be expressed as

$$|A_i| = \frac{A_{ix}}{\sqrt{1 + (f_L/f)^2}}, \quad (36)$$

and the phase of the current gain is

$$\phi_{A_i} = \tan^{-1} \left(\frac{f_L}{f} \right). \quad (37)$$

From (36), it can be observed that for $f \approx 0$, the current gain is ~ 0 . Similarly, at $f > f_L$, then for any $k \leq 1$

$$|A_i| = A_i(\infty) = A_{ix} = kn. \quad (38)$$

In summary, for the perfectly coupled case where $k = 1$, (33) reduces to

$$A_{ix} \simeq A_{i\text{ideal}} = n, \quad (39)$$

and, in general, the expression in (33) can be used to determine the current gain of the transformer for any value of $k \leq 1$. From (34), it can be seen that the lower-cut-off frequency ω_L determines the range of frequencies, where a constant current conversion can be achieved. For transformers with a lower value of k , the BW, where the current gain is constant can be increased by adopting a transformer with a higher turns ratio. This argument is true for improving the magnitude of the current gain also.

3.3 Voltage gain

Fig. 2b shows the equivalent circuit to determine the voltage gain of the non-ideal transformer. The voltage across the reflected load impedance is

$$nv_o = \frac{Z_L}{Z_L + Z_s} v_{Lm}. \quad (40)$$

Similarly, the voltage across the magnetising inductance is expressed as

$$v_{Lm} = \frac{Z_m \parallel [n^2(Z_s + Z_L)]}{Z_p + Z_m \parallel [n^2(Z_s + Z_L)]} v_i. \quad (41)$$

Substituting (41) into (40), we get the non-ideal transformer voltage gain as

$$\begin{aligned} A_v &= \frac{v_o}{v_i} = \frac{1}{n} \left(\frac{Z_L}{Z_L + Z_s} \right) \frac{Z_m \parallel [n^2(Z_s + Z_L)]}{Z_p + Z_m \parallel [n^2(Z_s + Z_L)]} \\ &= \frac{nZ_L Z_m}{n^2(Z_s + Z_L)(Z_p + Z_m) + Z_p Z_m}. \end{aligned} \quad (42)$$

Substituting (9)–(12) into (42), we obtain the expression for the voltage transfer function of the non-ideal transformer in terms of the circuit components as (see (43))

yielding

$$A_v = \frac{knR_L}{L_p(1-k^2)} \frac{s}{s^2 + \frac{r_p + n^2(r_s + R_L)}{L_p(1-k^2)} + \frac{n^2 r_p(r_s + R_L)}{(1-k^2)L_p^2}}. \quad (44)$$

The expression in (43) is a second-order transfer function of the transformer for resistive loads due to the two independent inductances. By expressing all the inductances in terms of L_p , the voltage transfer function can be modified into the standard-second-order form and is given by

$$A_v = A_{vx} \frac{s}{s^2 + 2\xi\omega_0 s + \omega_0^2}, \quad (45)$$

where A_{vx} is the high-frequency voltage gain

$$A_{vx} = \frac{knR_L}{L_p(1-k^2)}, \quad (46)$$

$$A_v = \frac{\frac{nsL_m R_L}{n^2(L_{lp}L_{ls} + L_m L_{ls}) + L_m L_{lp}}}{s^2 + \left[\frac{n^2(r_p L_{ls} + r_s L_{lp} + r_s L_m + R_L L_m + R_L L_{lp}) + r_p L_m}{n^2(L_{lp}L_{ls} + L_m L_{ls}) + L_m L_{lp}} \right] s + \frac{n^2 r_p(r_s + R_L)}{n^2(L_{lp}L_{ls} + L_m L_{ls}) + L_m L_{lp}}}, \quad (43)$$

the undamped natural frequency ω_0 is

$$\omega_0 = \frac{n}{L_p} \sqrt{\frac{r_p(r_s + R_L)}{1 - k^2}}, \quad (47)$$

and the damping ratio ξ is

$$\xi = \frac{r_p + n^2(r_s + R_L)}{2n\sqrt{(1 - k^2)[r_p(r_s + R_L)]}}. \quad (48)$$

The expression in (45) can be modified to obtain a transfer function with well-separated real poles as

$$A_v = A_{vx} \frac{s}{s^2 + (\omega_{Lv} + \omega_{Hv})s + \omega_{Lv}\omega_{Hv}} = A_{vx} \frac{s}{(s + \omega_{Lv})(s + \omega_{Hv})}, \quad (49)$$

where ω_{Lv} and ω_{Hv} are the lower- and upper-cut-off frequencies of the transformer voltage transfer function, respectively. Comparing (45) with (49), $2\xi\omega_0 = \omega_{Lv} + \omega_{Hv}$ and $\omega_0 = \sqrt{\omega_{Lv}\omega_{Hv}}$. The expressions for the cut-off frequencies in terms of ξ and ω_0 can be determined as

$$\omega_{Hv}, \omega_{Lv} = 2\pi f_{Hv}, 2\pi f_{Lv} = \xi\omega_0 \pm \omega_0\sqrt{\xi^2 - 1}, \quad (50)$$

Substituting for ω_0 and ξ in (47) and (48) into (50), we get (see (51))

Using the expressions for f_{Hv} and f_{Lv} , the transformer BW is

$$\begin{aligned} \text{BW} &= f_{Hv} - f_{Lv} \\ &= \frac{\sqrt{[r_p + n^2(r_s + R_L)]^2 - 4n^2(1 - k^2)[r_p(r_s + R_L)]}}{2\pi L_p(1 - k^2)}. \end{aligned} \quad (52)$$

For a perfectly coupled case, where $k=1$, the BW is infinite. For any other value of $k < 1$, the BW reduces with k . In a lossless transformer, where $r_p = r_s = 0$, the lower-cut-off frequency f_{Lv} approaches 0. The upper-cut-off frequency is

$$f_{Hv} = \frac{n^2 R_L}{2\pi L_p(1 - k^2)}, \quad (53)$$

and the BW is $\text{BW} \simeq f_{Hv}$. This indicates that the lower-cut-off frequency is strongly dependent on the winding dc resistances, whereas the upper-cut-off frequency and the BW are governed by turns ratio n , load resistance R_L , primary self-inductance L_p , and the coupling coefficient k . Consider the standard-second-order transfer function in (45). Substituting $s = j\omega$ into (45), one obtains

$$A_v = A_{vx} \frac{j\omega}{(\omega_0^2 - \omega^2) + j(2\xi\omega_0)\omega} = \frac{A_{vx}}{2\xi\omega_0 + j\omega_0((\omega/\omega_0) - (\omega_0/\omega))}. \quad (54)$$

Further manipulation leads to

$$\begin{aligned} A_v &= \frac{A_{vx}}{2\xi\omega_0} \frac{1}{1 + (j/2\xi)((\omega/\omega_0) - (\omega_0/\omega))} \\ &= \frac{A_{v0}}{1 + (j/2\xi)((\omega/\omega_0) - (\omega_0/\omega))}, \end{aligned} \quad (55)$$

where A_{v0} is the maximum voltage gain for the mid-frequency region

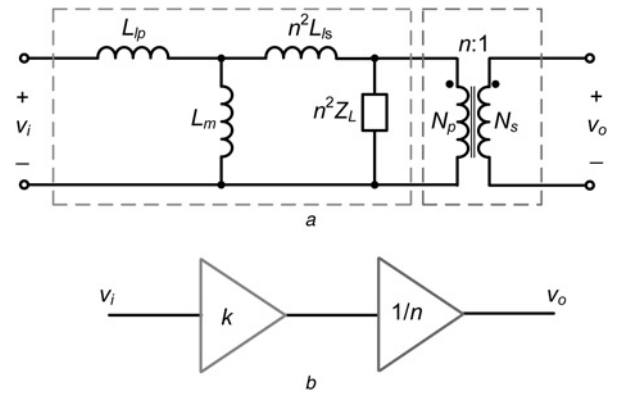


Fig. 3 Transformer model and its equivalent gain stages

a Equivalent model of the transformer neglecting the winding dc resistances
b Representation of the voltage gain transfer function in the mid-frequency region in terms of gain stages

and is given as

$$A_{v0} = \frac{A_{vx}}{2\xi\omega_0} = \frac{knR_L}{r_p + n^2(r_s + R_L)}. \quad (56)$$

The magnitude of the voltage gain is

$$|A_v| = \frac{A_{v0}}{\sqrt{1 + \left(\frac{1}{4\xi^2}\right)\left[\left(\frac{\omega}{\omega_0}\right) - \left(\frac{\omega_0}{\omega}\right)\right]^2}}, \quad (57)$$

and the phase of the voltage gain is

$$\phi_{A_v} = -\tan^{-1}\left[\frac{1}{2\xi}\left(\frac{\omega}{\omega_0} - \frac{\omega_0}{\omega}\right)\right]. \quad (58)$$

Thus, at $\omega = \omega_0 = \sqrt{\omega_{Lv}\omega_{Hv}}$, the magnitude of the voltage gain becomes

$$|A_v| = A_{v0} = \frac{knR_L}{r_p + n^2(r_s + R_L)}, \quad (59)$$

whereas for $\omega \rightarrow 0$ and $\omega \rightarrow \infty$, the $|A_v|$ approaches zero. The expressions for voltage gain in (45) and (59) are applicable for any $k \leq 1$. Consider the case of an ideal transformer, where $r_p = r_s = 0$ and $k=1$ such that $L_{lp} = L_{ls} = 0$ and $L_m = \infty$, then (59) reduces to

$$|A_v| \simeq A_{v0} = A_{v\text{ideal}} = \frac{1}{n}. \quad (60)$$

For any other value of $k < 1$, the inductances have a finite value. If $r_p = r_s = 0$, then (59) reduces to

$$A_v \simeq A_{v0} = kA_{v\text{ideal}} = \frac{k}{n}, \quad (61)$$

indicating that the effective voltage gain of the transformer is equal to a fraction k of the voltage gain of the ideal transformer. Therefore, the equivalent model of the transformer can be represented as a product of the coupling coefficient and the turns ratio of the ideal transformer and the effect is depicted in Fig. 3. This result is validated in Section 5.

$$f_{Hv}, f_{Lv} = \frac{r_p + n^2(r_s + R_L) \pm \sqrt{[r_p + n^2(r_s + R_L)]^2 - 4n^2(1 - k^2)[r_p(r_s + R_L)]}}{4\pi L_p(1 - k^2)}. \quad (51)$$

4 Transformer efficiency

4.1 Transformer efficiency as a function of frequency

It is well known that the useful energy is accomplished using the real power. Therefore, it is essential to deduce an equation for the transformer efficiency to determine the effectiveness of power transfer at different values of coupling coefficient. The real output power of the transformer is

$$P_o = \frac{1}{2} V_{om} I_{om} \cos(\phi_{v_o} - \phi_{i_o}) = \frac{1}{2} V_{om} I_{om} \cos(\phi_{z_o}). \quad (62)$$

If the transformer is loaded by a resistance, then $\phi_{z_o} = 0$ and $V_{om} = I_{om} R_L$. Thus, the output power is

$$P_o = \frac{1}{2} (I_{om} R_L) I_{om} \cos(0) = \frac{1}{2} I_{om}^2 R_L. \quad (63)$$

Similarly, the real input power of the transformer is

$$P_i = \frac{1}{2} V_{im} I_{im} \cos(\phi_{v_i} - \phi_{i_i}) = \frac{1}{2} V_{im} \cos(\phi_{z_i}) I_{im}. \quad (64)$$

In this case, the equivalent input voltage $V_{im} \cos(\phi_{z_i})$ appears across the real part of the input impedance $R_i = \text{Re}(Z_i)$ such that the input voltage $V_{im} \cos(\phi_{z_i}) = I_{im} R_i$. The value of the input resistance R_i can be determined from (15). Thus, the real input power is expressed as

$$P_i = \frac{1}{2} (I_{im} R_i) I_{im} = \frac{1}{2} I_{im}^2 R_i. \quad (65)$$

The transformer efficiency η_t with resistive loads is the ratio of the real output power in (63) to the real input power in (65) and is given by

$$\eta_t = \frac{P_o}{P_i} = \frac{I_{om}^2 R_L}{I_{im}^2 R_i} = A_{ix}^2 \frac{R_L}{R_i}. \quad (66)$$

where $A_{ix} = |A_i|$ is the magnitude of the current gain at mid-frequencies and can be obtained from (32). By substituting for R_i and A_{ix} in (23) and (38), respectively, into (66), the transformer efficiency as a function of frequency can be expressed as

$$\eta_t = \frac{(kn)^2 R_L \left[1 + \left(\omega_p / \omega \right)^2 \right]}{r_p \left[1 + \left(\omega_p / \omega \right)^2 \right] - Z_x(\omega_p - \omega_z)}. \quad (67)$$

As $\omega \rightarrow \infty$, the term ω_p / ω approaches zero resulting in the transformer efficiency at mid-frequencies as

$$\eta_t = \frac{(kn)^2 R_L}{r_p - Z_x(\omega_p - \omega_z)}. \quad (68)$$

Substituting for ω_z and ω_p in (18) and (19), respectively, into (68), we get the mid-frequency transformer efficiency as

$$\eta_t = \frac{(kn)^2 R_L}{r_p + (kn)^2 (r_s + R_L)} = \frac{1}{1 + (1/(kn)^2)(r_p/R_L) + (r_s/R_L)}. \quad (69)$$

For example, at $R_L = 0.2 \Omega$, $n = 1.4$, $r_p = 0.02 \Omega$, and $r_s = 0.015 \Omega$, the transformer efficiency is $\eta_t = 0.888$ at $k = 1$. However, as k is reduced to 0.2, the efficiency is reduced to 0.4254. Thus, as the coupling coefficient is lowered at a fixed load resistance, the transformer efficiency also reduces drastically. The transformer

efficiency is degraded as the value of the load resistance becomes comparable with the winding dc resistances.

4.2 Transformer efficiency at mid-frequencies in terms of power losses

An alternate approach to the above analysis to determine the maximum efficiency at mid-frequencies is presented in this section. If the power loss across the priming winding dc resistance is $P_{rp} = I_{im}^2 r_p / 2$ and the power loss across the secondary winding dc resistance is $P_{rs} = I_{om}^2 r_s / 2$, the total power loss in the two winding dc resistances is

$$P_{ls} = \frac{I_{im}^2 r_p}{2} + \frac{I_{om}^2 r_s}{2}. \quad (70)$$

In terms of the power loss and the output power, the transformer efficiency is

$$\eta_t = \frac{P_o}{P_o + P_{ls}} = \frac{1}{1 + (P_{ls}/P_o)}. \quad (71)$$

Substituting (63) and (70) into (72), we obtain

$$\eta_t = \frac{1}{1 + \left[(I_{im}^2 r_p + I_{om}^2 r_s) / (I_{om}^2 R_L) \right]} = \frac{1}{1 + (1/A_{ix}^2)(r_p/R_L) + (r_s/R_L)}, \quad (72)$$

where $A_{ix} = |A_i| = I_{om}/I_{im}$. Substituting $|A_{ix}| = kn$ into (72), we get the transformer efficiency as

$$\eta_t = \frac{1}{1 + [1/(kn)^2](r_p/R_L) + (r_s/R_L)}. \quad (73)$$

The expressions in (73) and (69) are identical and either may be used to determine the maximum achievable efficiency. It can be seen from (73) that under ideal circumstances, where $k = 1$, $r_p = r_s = 0$, the value of $\eta_t = 1$. The transformer efficiency decreases significantly with decreasing coupling coefficient. In addition, the efficiency also reduces as the values of the load resistance and the dc winding resistances become comparable. For example, at $k = 0.5$, $n = 1.4$, $r_p = 0.02 \Omega$, and $r_s = 0.015 \Omega$, the transformer efficiency is $\eta_t = 0.99$ at $R_L = 20 \Omega$. However, as R_L is decreased to 0.2Ω , the efficiency reduces to 0.84.

5 Results

This section analyses the expressions for the voltage gain, current gain, input impedance, and the efficiency of the non-ideal transformer derived in Sections 3 and 4 and provides the simulation and experimental results.

5.1 Transformer design

To present the analysis, a transformer with the following specifications was designed, simulated, built, and tested:

- Number of turns of primary winding $N_p = 14$.
- Number of turns of secondary winding $N_s = 10$.
- Turn ratio $n = N_p/N_s = 1.4$.
- Magnetic core – 0P43622UG (DS pot core).
- Relative permeability of the magnetic core material $\mu_{rc} = 2500$.
- Core cross-sectional area A_c of each of the two core halves = 202 mm^2 .
- Mean magnetic path length $l_c = 53.2 \text{ mm}$.
- Mean turn length $l_T = 72.72 \text{ mm}$.

- Primary and secondary windings wire – American Wire Gauge (AWG)-18 with inner wire diameter $d_w = 1.02362$ mm.

Detailed design procedure is provided in [1, 2, 31–42]. Using (3) and (4), the primary and secondary self-inductances L_p and L_s are determined as

$$\begin{aligned} L_p &= \frac{\mu_0 \mu_r A_c N_p^2}{l_c} \\ &= \frac{4\pi \times 10^{-7} \times 2500 \times 202 \times 10^{-6} \times 14^2}{53.2 \times 10^{-3}} \text{ H} \\ &= 2.337 \text{ mH} \end{aligned} \quad (74)$$

and

$$\begin{aligned} L_s &= \frac{\mu_0 \mu_r A_c N_s^2}{l_c} \\ &= \frac{4\pi \times 10^{-7} \times 2500 \times 202 \times 10^{-6} \times 10^2}{53.2 \times 10^{-3}} \text{ H} \\ &= 1.192 \text{ mH} \end{aligned} \quad (75)$$

The length of the primary winding wire l_{wp} and the length of the secondary winding wire l_{ws} , respectively, are

$$l_{wp} = N_p l_T = 14 \times 72.72 \times 10^{-3} \text{ m} = 1018.08 \text{ mm} \quad (76)$$

and

$$l_{ws} = N_s l_T = 10 \times 72.72 \times 10^{-3} \text{ m} = 727.2 \text{ mm} \quad (77)$$

To accommodate the leads for the primary and secondary winding wire connections, let $l_{wp} = 1030$ mm and $l_{ws} = 740$ mm. Given that the resistivity of copper (Cu) conductor is $\rho_{Cu} = 1.724 \times 10^{-8} \Omega\text{m}$ at room temperature ($T = 20^\circ\text{C}$) and the inner area of the AWG-18 Cu wire is $A_w = \pi d_w^2 / 4 = 0.8225 \text{ mm}^2$. The dc and low-frequency wire resistance of the primary winding is

$$r_p = \frac{\rho_{Cu} l_{wp}}{A_w} = \frac{1.724 \times 10^{-8} \times 1030 \times 10^{-3}}{0.8225 \times 10^{-6}} \Omega = 21.6 \text{ m}\Omega \quad (78)$$

and the dc and low-frequency wire resistance of the secondary winding is

$$r_s = \frac{\rho_{Cu} l_{ws}}{A_w} = \frac{1.724 \times 10^{-8} \times 740 \times 10^{-3}}{0.8225 \times 10^{-6}} \Omega = 15.51 \text{ m}\Omega \quad (79)$$

The load resistance is fixed at $R_L = 22 \Omega$. For these values, the input impedance, current gain, and the voltage gain were analysed and the results are presented in the subsequent sections.

5.2 SABER simulation results

For the given specifications, the transformer was built on SABER circuit simulator using the Model Architect tool. It was assumed that the permeability of the core material and the winding dc resistance are frequency-independent, i.e. these parameters have constant values up to the high-frequency region. The validity of these assumptions is tested in this section using the Model Architect tool. The Model Architect hosts a series of applications including the tool for magnetic component characterisation (MCC). The MCC tool is dedicated to the design of inductors and transformers, to determine their magnetic and electrical properties, to estimate power losses, impedances, and also contains the coil geometry optimisation tool. In view of this work, the MCC is capable of providing information about the effective relative permeability, ac resistance, and core losses. The effective relative

permeability μ_{re} is expressed as

$$\mu_{re} = \frac{\mu_{rc}}{1 + \mu_{rc}(l_g/l_c)}, \quad (80)$$

where l_g is the length of the air gap. As shown in Fig. 4a, the value of μ_{re} is constant up to 100 kHz and is equal to $\mu_{rc} = 2500$. A reduction in the value of the core permeability was observed at frequencies beyond 1 MHz due to the ferromagnetic resonance phenomenon within the core structure [1]. Since the frequency of interest in this paper is <1 MHz, the assumption that the effect of the permeability on the transfer functions is negligible is valid.

Similarly, the ac resistance R_{ac} of the transformer was determined through simulations and the plot of the input ac resistance as a function of frequency is as shown in Fig. 4b. At dc ($f=0$), the input resistance has a value approximately equal to $r_p = 20 \text{ m}\Omega$. Though the value of the resistance increases with frequency, it was realised by the authors that the increment is small, when compared with the value of the load resistance R_L , and does not affect the characteristics of the transfer functions, especially within the frequency range of interest.

5.3 Theoretical results obtained using MATLAB

The plots for the variation in the input resistance for different values of the coupling coefficient as a function of frequency are shown in Fig. 5a. For $k=1$, the input impedance is dominated by the input resistance component. Thus, the input impedance increases from r_p to a value equal to $r_p + n^2(r_s + R_L)$, which is in accordance with (24) and (25). For any other value of $k < 1$, the maximum input resistance can be obtained using (25). Fig. 5b shows the variation in the input inductance as a function of frequency for different values of the coupling coefficient. At dc, the input inductance L_i given in (29) is equal to the self-inductance L_p of the primary winding for each value of the coupling coefficient. However, for $k \approx 1$, as the frequency increases, the input inductance approaches zero.

The plots for variations in the magnitude and phase of the input impedance as a function of frequency for different values of the coupling coefficient plotted using MATLAB are shown in Figs. 5c and 5d, respectively. However, for $k < 1$, the input reactance in the mid-frequency range dominates the input resistance. Thus, the input impedance is inductive in the mid-frequency range and beyond and is indicated in (26) and (28). The phase plot of the input impedance illustrates the effect of (22). For $k=1$, at dc, $X_i = 0$, resulting in $\phi_{Z_i} = 0$, whereas, when $\omega \rightarrow \infty$, $R_i > X_i$, leading to $\phi_{Z_i} = 0$. For any other value of $k < 1$, ϕ_{Z_i} is $\sim 90^\circ$ throughout the frequency range. At lower values of k , the reactance due to the primary leakage inductance becomes stronger and its value increases with frequency. Thus, a proper technique to nullify the leakage inductance at lower k must be employed in order to maximise the transfer of real power.

The plots for variations in the magnitude and phase of the current gain as a function of frequency for different values of the coupling coefficient plotted using MATLAB are shown in Figs. 6a and 6b, respectively. Consider the case when $k=0.6$. The magnitude plot shows the characteristics of a high-pass filter with a maximum current gain A_{ix} and a lower-cut-off frequency $f_L = \omega_L / 2\pi$. The values of A_{ix} and ω_L are derived in (33) and (34), respectively. From the plot of the magnitude of the current gain, it can be observed that the coupling coefficient has no effect on the lower-cut-off frequency. In the mid-frequency range, i.e. $f > f_L$, using (38), it can be stated that the maximum current gain A_{ix} is no longer equal to simply n for any $k < 1$. Thus, if $A_{i,ideal} = n = 1.4$ and $k = 0.6$, then the effective turns ratio is $1.4 \times 0.6 = 0.84$ or has reduced by $\sim 60\%$ of the ideal value. This value coincides with the maximum value of A_i in Fig. 6a. Fig. 6b shows that the phase plot for each of the coupling coefficient is the same. The transformer offers a phase difference of 90° between the input and output currents at low frequencies. For all frequencies beyond the lower-cut-off frequency, the phase shift reduces to zero.

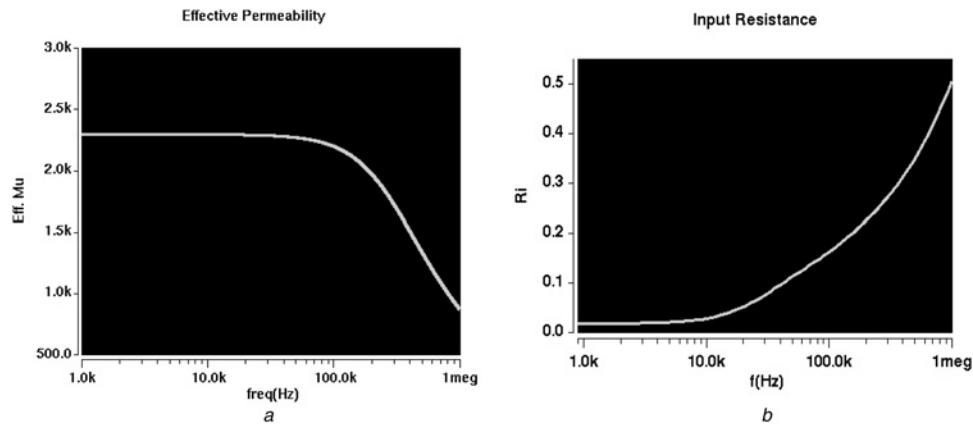


Fig. 4 Variation in the effective relative permeability μ_{re} and the ac resistance R_{ac} as a function of frequency obtained using SABER circuit simulator for the non-ideal transformer under consideration

a Effective permeability as a function of frequency
 b AC resistance as a function of frequency

The variations in the magnitude and phase of the voltage gain as a function of frequency for different values of the coupling coefficient are shown in Figs. 6c and 6d, respectively. The equation for the voltage gain represents the characteristics of a second-order band-pass filter with a lower-cut-off frequency f_{LV} , upper-cut-off frequency f_{HV} , and a maximum gain A_{v0} , whose expressions are

provided in (51) and (56). These equations determine the theoretical limits on the voltage gain and BW, which are achievable for any value of the coupling coefficient. On knowing these values, the transformer design can be optimised to ensure that the operating frequency exists within the BW required for the highest voltage gain. The lower-cut-off frequency is usually close

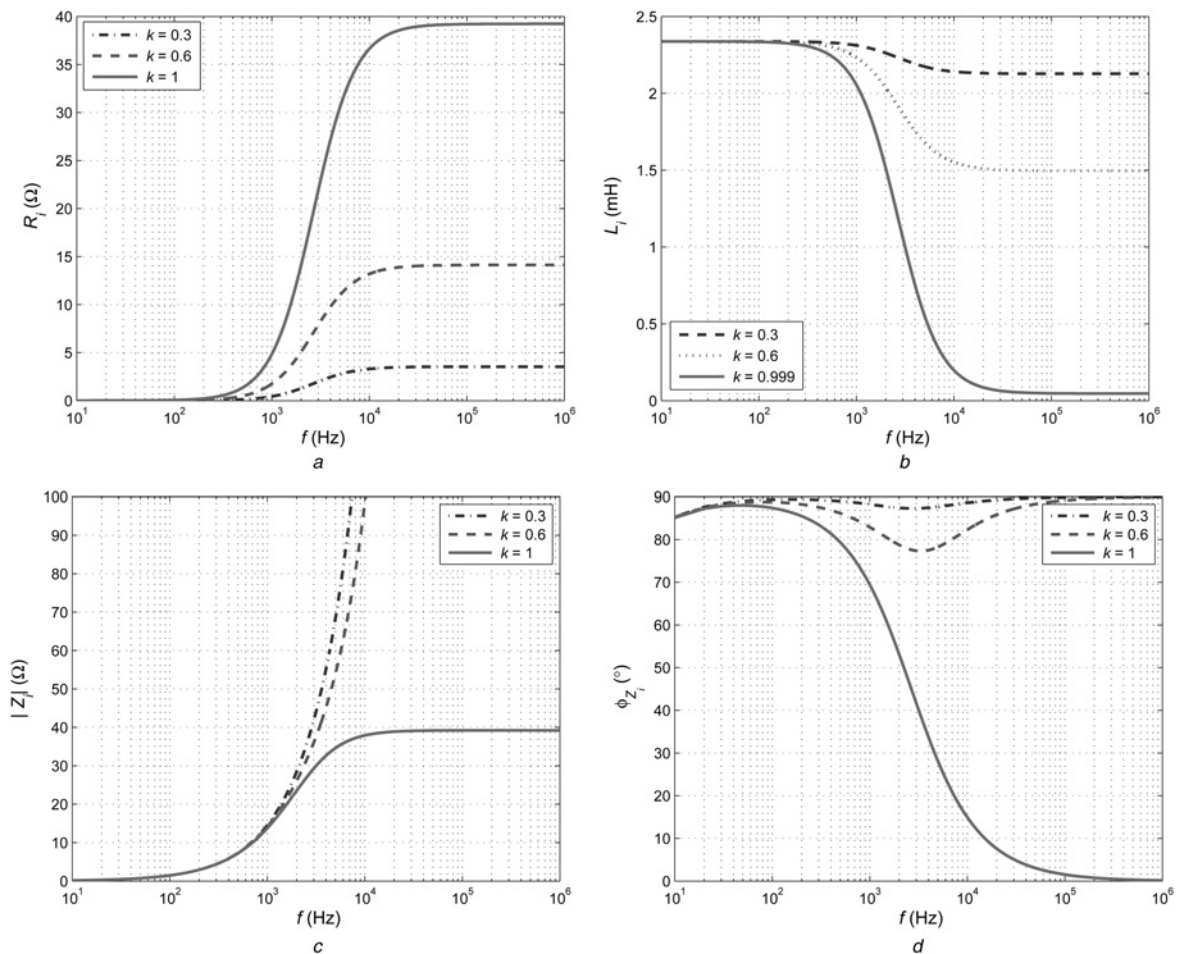


Fig. 5 Theoretically obtained plots of variations in the input resistance R_i , input inductance L_i , and magnitude and phase of the input impedance Z_i of the non-ideal transformer with change in frequency for different values of coupling coefficient

a Input resistance as a function of frequency
 b Input inductance as a function of frequency
 c Magnitude of the input impedance $|Z_i|$ as a function of frequency
 d Phase of the input impedance ϕ_{Z_i} as a function of frequency

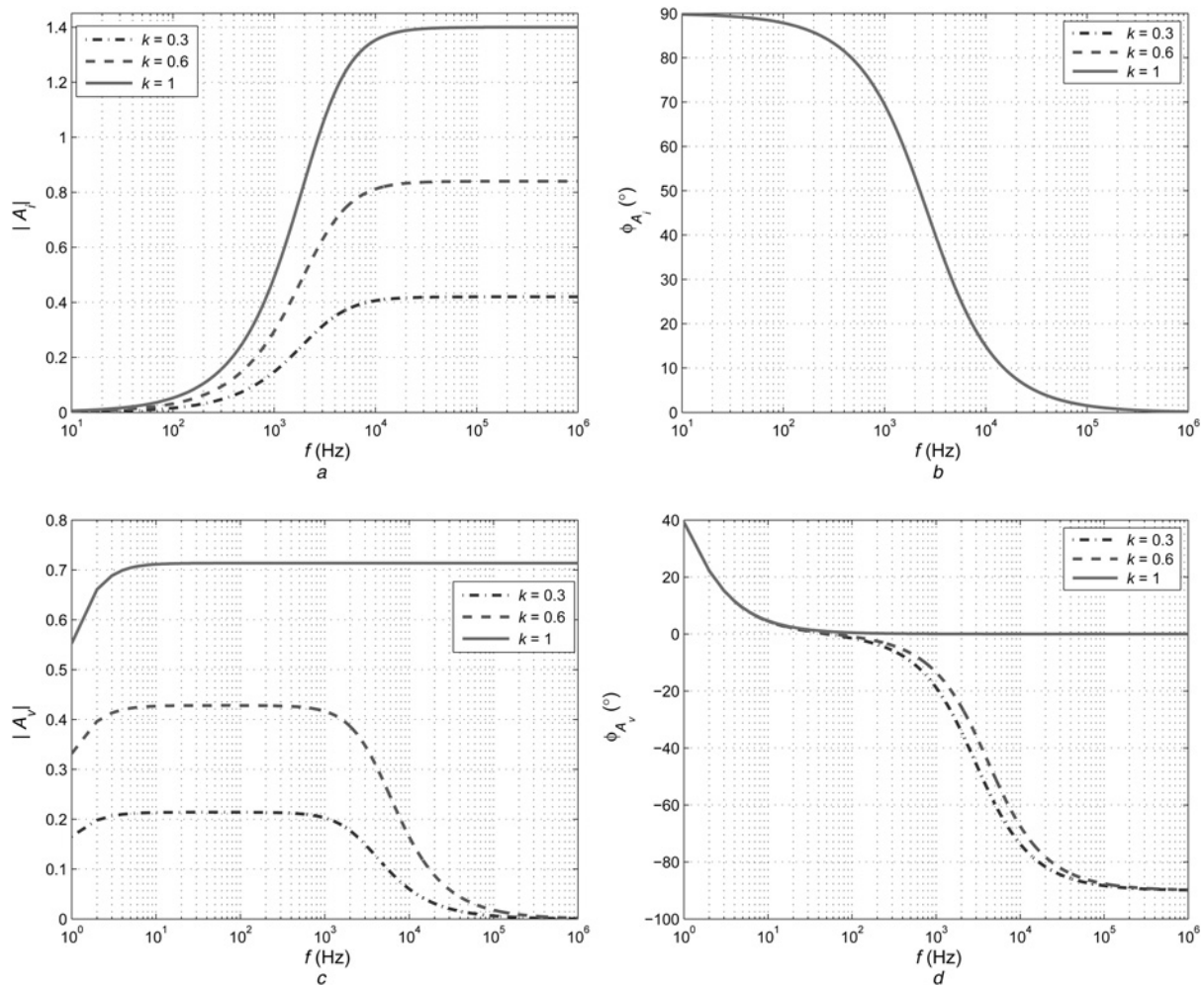


Fig. 6 Theoretically obtained plots of variations in the magnitude and phase of the current gain A_i and the voltage gain A_v of the non-ideal transformer with change in frequency for different values of coupling coefficient

- a Magnitude of the current gain $|A_i|$ as a function of frequency
b Phase of the current gain ϕ_{A_i} as a function of frequency
c Magnitude of the voltage gain $|A_v|$ as a function of frequency
d Phase of the voltage gain ϕ_{A_v} as a function of frequency

to zero and is dependent on the winding dc resistances, thus is not considered as a major criterion. However, the upper-cut-off frequency f_{Hv} determines the BW of the non-ideal transformer. Assuming that the transformer is ideal, such that $k=1$, $r_p=r_s=0$, then the voltage gain of the transformer is equal to $A_{v\text{ ideal}}=1/n=0.7143$. From Fig. 6c, for $k=0.6$, the maximum value of the voltage gain is $A_{v0}=0.4276$ as opposed to the ideal value of 0.7143. Therefore, due to the low coupling coefficient, the effective voltage gain is ~60% or equal to k times the ideal value $A_{v\text{ ideal}}$ for frequencies up to the upper-cut-off frequency $f_{Hv}=4.24$ kHz. This value for the BW coincides with that calculated using (53). The phase of the voltage transfer function is 90° at frequencies less than $f_0=\omega_0/2\pi$ for any value of k . For $k=1$, the voltage drop across the leakage inductances is zero and the phase is 0 at any frequency $f \geq f_0$. However, for any $k < 1$, the leakage inductances are dominant at high-frequencies resulting in a -90° phase difference between the output and input voltages.

The efficiency of the transformer with resistive loads as given in (67) is plotted as a function of frequency as shown in Fig. 7a. The magnitude of the efficiency is lower than one for all values of $R_i > R_L$, where R_i is the input resistance of the transformer and R_L is the load resistance. However, for $R_i=R_L$, then the efficiency approaches unity indicating a maximum power transfer from the source to the load. Fig. 7b shows the variation in the efficiency as a function of the coupling coefficient at different load resistances for $n=1.4$. At lower values of load resistance, which are comparable

with the values of the dc winding resistances, the transformer efficiency at any coupling coefficient is also reduced due to higher conduction losses. However, when the load resistance is higher than the dc winding resistance, then transformer efficiency is low only at lower values of k , but approaches unity as $k \rightarrow 1$.

5.4 Experimental results

For the given specifications, the transformer was constructed using the cores and winding specified in Section 5.1. Fig. 8a shows the photograph of the transformer, which was built and used for measurements. A non-inductive resistor of value $R_L=20\ \Omega$ was used. The primary and secondary inductances were measured using the HP 4275A multi-frequency impedance meter. The self-inductance of the primary winding L_p was 2.19 mH and the self-inductance of the secondary winding L_s was 1.21 mH, when perfectly coupled. The equivalent series resistances or the winding dc resistances at the primary and secondary were measured as $r_p=0.022\ \Omega$ and $r_s=0.017\ \Omega$, respectively. The experiment was first executed by adjusting the gap to get a coupling coefficient of $k=0.98$. The coupling coefficient k for the transformer was calculated using [38]

$$k = \sqrt{1 - \frac{L_p'}{L_p}}, \quad (81)$$

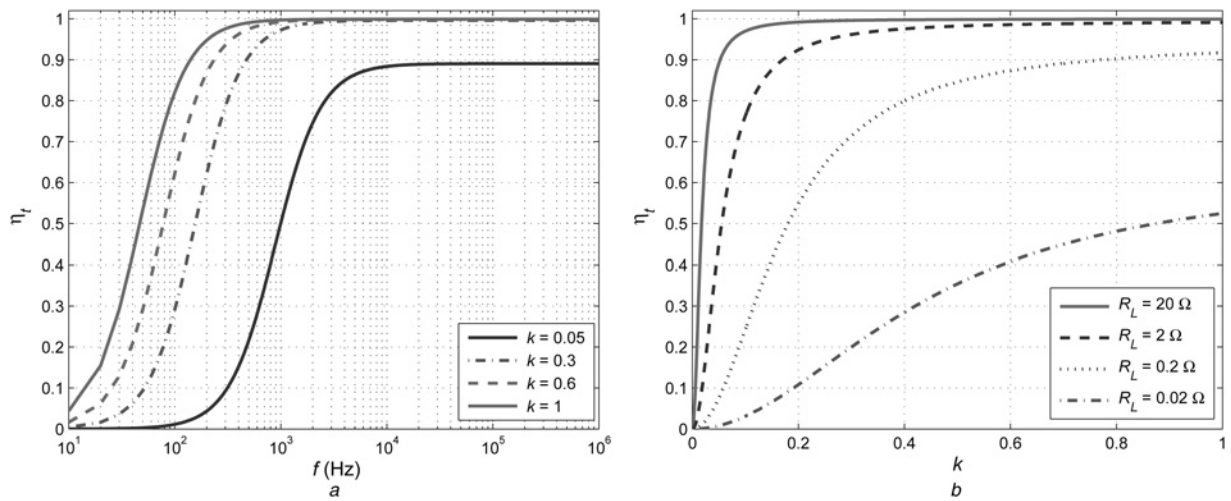


Fig. 7 Theoretically obtained plots of variations in the transformer efficiency with change in frequency and coupling coefficient
a Variation in the transformer efficiency given in (66) for resistive loads with change in frequency for different values of coupling coefficient at $R_L = 22 \Omega$
b Variation in the mid-frequency transformer efficiency as a function of the coupling coefficient for different values of load resistance at $n = 1.4$

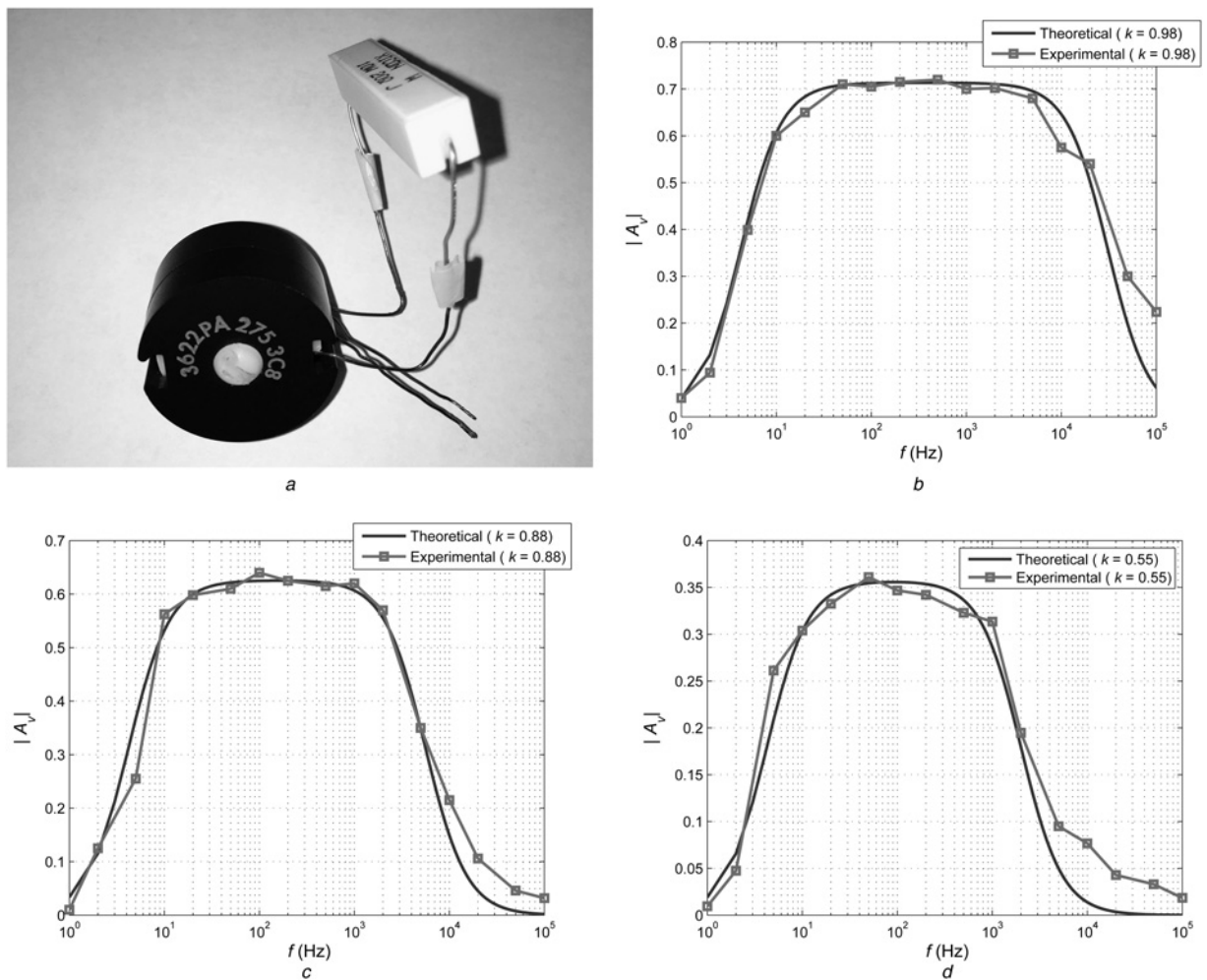


Fig. 8 Photograph of the experimental set-up and comparison of theoretical and experimental results for the magnitude of the voltage gain of the non-ideal transformer

- a* Photograph of the transformer used for measurements
- b* Theoretical and experimental voltage gain at $k = 0.98$
- c* Theoretical and experimental voltage gain at $k = 0.88$
- d* Theoretical and experimental voltage gain at $k = 0.55$

where L_p' represents the measured inductance at the primary when the secondary winding is short circuited and L_p is the measured inductance at the primary when the secondary winding is open circuited. For an input voltage of 1 V, the output voltage was measured at different frequencies between 10 Hz and 1 MHz.

Fig. 8b illustrates the comparison of the theoretical and experimental results for the magnitude of the voltage gain A_v of the transformer at a coupling coefficient of $k=0.98$. At low frequencies, the values of the reactive components are low and the parasitic resistance of the measurement components becomes significant. Thus, a careful estimation of the probe and component parasitics must be made. The two results were in accordance with each other in the dc and mid-frequency range. Furthermore, the transformer winding arrangement was adjusted to obtain lower values of coupling coefficients. Again using (81), the new coupling coefficient was found to be $k \approx 0.8$. The experiment was repeated and the result is as shown in Fig. 8c. The results were in fair agreement in the useful range of frequencies. Another set of measurements were obtained for $k \approx 0.55$. The theoretically predicted and experimental results matched very well at dc, low-, and mid-frequencies. A deviation in the experimental results from the theoretical predictions was observed at frequencies beyond 50 kHz at the three coupling coefficients. The following practical reasons, which have been neglected in this analysis, could be attributed for the mismatch at high-frequencies:

- The core and winding equivalent series resistances may become significant at $f > 50$ kHz and cause the roll-off slope of the voltage gain plot to decrease.
- The parasitics of the transformer such as turn-to-turn capacitance, inter-winding capacitance, winding-to-core capacitance etc., alters the shape of the voltage gain curve.
- The probe capacitance and the lead inductance of the load resistor.

6 Conclusion

In this paper, the closed-form expressions for the following characteristics of a non-ideal transformer with a resistive load have been derived as functions of frequency at different values of the coupling coefficient: input impedance Z_i , current gain A_i , voltage gain A_v , $BW = f_{HV} - f_{LV}$, and transformer efficiency η_t . The magnetising inductance, leakage inductances, and dc resistances of the primary and secondary windings have been taken into account. The parasitic capacitances and the core resistance are neglected. A general conclusion is that the coupling coefficient has a significant effect on the input resistance, current gain, voltage gain, and the transformer efficiency. The main conclusions drawn from the analysis and experiments of this paper are as follows:

- The transformer input impedance Z_i is governed by its input resistance R_i and input inductance L_i . For a transformer with a fixed load resistance R_L , as the frequency increases from zero, the input resistance R_i increases from a minimum value r_p to a maximum value $(kn)^2(r_s + R_L)$, where k is the coupling coefficient, and r_p and r_s are the primary and secondary windings dc resistances, respectively. The input inductance L_i is equal to the self-inductance L_p of the primary winding at dc at any value of k , while its value decreases with increase in frequency as given in (29). At mid-frequencies, the input inductance approaches zero for $k=1$, while as k is reduced to zero, L_i approaches L_p .
- The current gain A_i of the non-ideal transformer is similar to the transfer function of a first-order high-pass filter. As the frequency increases from zero, the magnitude of the current gain $|A_i|$ increases from zero to kn .
- The voltage gain A_v resembles a second-order band-pass filter transfer function for $k < 1$ and as a high-pass filter transfer function for $k=1$. The maximum value of the voltage gain A_{v0} given in (59) is not only equal to $1/n$, but is a function of the coupling coefficient, dc winding resistances, and load resistance. For a lossless transformer, the maximum value of voltage gain is $A_{v0} \approx kn$.

(iv) The lower-cut-off frequency f_{LV} of the voltage gain A_v is dependent on the winding dc resistances and is ~ 0 if the dc resistances are small compared with R_L . The upper-cut-off frequency f_{HV} of the voltage gain determines the BW and depends primarily on the load resistance R_L , primary self-inductance L_p , and coupling coefficient k as given in (53). The transformer BW decreases as the coupling coefficient is reduced.

(v) The expression for the transformer efficiency η_t as a function of frequency for any value of k has been derived and is given in (67). As the frequency increases from zero, the transformer efficiency η_t at each coupling coefficient k also increases to a maximum value given in (69).

(vi) The transformer efficiency η_t reduces with the coupling coefficient. At mid-frequencies, the η_t decreases as the ratios r_p/R_L or r_s/R_L increases and is determined in (73).

The design of a non-ideal transformer for practical specifications has been presented. The theoretically obtained results have been investigated using MATLAB and SABER simulation tools. A laboratory set-up comprising of the designed transformer with a facility to adjust the coupling coefficient has been built. The experimental results have proved the validity of the theoretical predictions over a wide range of test frequencies.

Future work in this regard constitutes the analysis of the transformer in the presence of parasitic capacitance, frequency-dependent magnetic permeability, and winding resistances. The expressions provided in this paper can be used in designing reactive compensation networks for a achieving maximum power transfer.

7 References

- Kazimierzczuk, M.K.: 'High-frequency magnetic components' (John Wiley and Co., Chichester, UK, 2014, 2nd edn.)
- den Bossche, A.V., Valchev, V.C.: 'Inductors and transformers for power electronics' (CRC Press, FL, USA, 2005)
- McLyman, C.W.T.: 'Transformer and inductor design handbook' (Marcel Dekker, New York, NY, 2004, 3rd edn.)
- Ayachit, A., Kazimierzczuk, M.K.: 'Thermal effects on inductor winding resistance at high frequencies', *IEEE Magn. Lett.*, 2013, **4**, (1)
- Witliski, A.F.: 'Introduction to modeling of transformers and coupled inductors', *IEEE Trans. Power Electron.*, 1995, **10**, (3), pp. 349–357
- Lopera, J.M., Prieto, M.J., Pernia, A.M., et al.: 'A multiwinding modeling method for high frequency transformers and inductors', *IEEE Trans. Power Electron.*, 2003, **18**, (3), pp. 896–906
- Youssef, M.Z., Jain, P.K.: 'Series-parallel resonant converter in self-sustained oscillation mode with the high-frequency transformer-leakage-inductance effect: analysis, modeling, and design', *IEEE Trans. Ind. Electron.*, 2007, **54**, (3), pp. 1329–1341
- Liu, X., Wang, G., Ding, W.: 'Efficient circuit modelling of wireless power transfer to multiple devices', *IET Power Electron.*, 2014, **7**, (12), pp. 3017–3022
- Musavi, F., Eberle, W.: 'Overview of wireless power transfer technologies for electric vehicle battery charging', *IET Power Electron.*, 2014, **7**, (1), pp. 60–66
- Sanghoon, C., Yon-Hae, K., Kang, S.-Y., et al.: 'Circuit-model-based analysis of a wireless energy-transfer system via coupled magnetic resonances', *IEEE Trans. Ind. Electron.*, 2010, **58**, (7), pp. 2906–2914
- Dalessandro, L., Cavalcante, F.S., Kolar, J.K.: 'Self-capacitance of high-voltage transformers', *IEEE Trans. Power Electron.*, 2007, **22**, (5), pp. 2081–2092
- Yu, X.J., Cheng, J.M.: 'Leakage inductance compensation for loosely coupled transformer considering parasitic resistance', *IET Electron. Lett.*, 2010, **46**, (10), pp. 717–719
- Hayano, S., Nakajima, Y., Saotome, H., et al.: 'A new type of high frequency transformer', *IEEE Trans. Magn.*, 1991, **27**, (6), pp. 5205–5207
- Kondrath, N., Kazimierzczuk, M.K.: 'Bandwidth of current transformer', *IEEE Trans. Instrum. Meas.*, 2009, **58**, (6), pp. 2008–2016
- Faiz, J., Abed-Ashtiani, B., Byat, M.R.: 'Lumped complete equivalent circuit of a coreless high-frequency transformer', *IEEE Trans. Magn.*, 1997, **33**, (1), pp. 703–707
- Greene, J.D., Gross, C.A.: 'Nonlinear modeling of transformers', *IEEE Trans. Ind. Appl.*, 1998, **24**, (3), pp. 434–438
- Boys, J.T., Covic, G.A., Yong, X.X.: 'Modeling and controller design of ICPT pick-ups', Proc. Int. Conf. Power System Technology, 2002, vol. 3, pp. 1602–1606
- Boys, J.T., Elliot, G.A.J., Covic, G.A.: 'An appropriate magnetic coupling co-efficient for the design and comparison of ICPT pickups', *IEEE Trans. Power Electron.*, 2007, **22**, (1), pp. 333–336
- Liu, C., Hu, A.P., Nair, N.-K.C.: 'Modelling and analysis of a capacitively coupled contactless power transfer system', *IET Power Electron.*, 2011, **4**, (7), pp. 808–815
- Dalessandro, L., Odendaal, W.G., Kolar, J.W.: 'HF characterization and non-linear modeling of a gapped toroidal magnetic structure', *IEEE Trans. Power Electron.*, 2006, **21**, (5), pp. 1167–1175

- 21 Boys, J.T., Covic, G.A., Green, A.W.: 'Stability and control of inductively coupled power transfer systems', *IEE Proc. Electr. Power Appl.*, 2009, **147**, (1), pp. 37–46
- 22 Boys, J.T., Covic, G.A., Elliott, G.A.J.: 'Pick-up transformer for ICPT applications', *IET Electron. Lett.*, 2002, **21**, (38), pp. 1276–1278
- 23 Myunghyo, R., Yonghwan, P., Juwon, B., *et al.*: 'Comparison and analysis of the contactless power transfer systems using the parameters of the contactless transformer'. Proc. IEEE Power Electronics Specialist Conf. Record, June 2006, pp. 1–6
- 24 Song, S., Liu, G., Gong, W., *et al.*: 'Electromagnetic analysis of a new magnetic core of transformer for a contactless electric vehicle charging'. Proc. Int. Conf. on Electrical Machines and Systems, August 2011
- 25 Lee, S.-H., Lorenz, R.D.: 'Development and validation of model for 95%-efficiency 220 W wireless power transfer over a 30 cm air gap', *IEEE Trans. Ind. Appl.*, 2011, **47**, (6), pp. 2495–2504
- 26 Ranstad, P., Nee, H.-P.: 'On the distribution of AC and DC winding capacitances in high-frequency power transformers with rectifier loads', *IEEE Trans. Ind. Electron.*, 2011, **58**, (5), pp. 1789–1798
- 27 Zierhofer, C.M., Hochmair, E.S.: 'Geometric approach for coupling enhancement of magnetic coupled coils', *IEEE Trans. Biomed. Eng.*, 1996, **43**, (7), pp. 708–714
- 28 Jegadeesan, R., Guo, Y.-X.: 'Topology selection and efficiency improvement of inductive power links', *IEEE Trans. Antennas Propag.*, 2012, **60**, (10), pp. 4846–4854
- 29 Dalessandro, L., Karrer, N., Kolar, J.W.: 'High-performance planar isolated current sensor for power electronics applications', *IEEE Trans. Power Electron.*, 2007, **22**, (5), pp. 1682–1692
- 30 Petkov, R.: 'Optimum design of a high-power, high-frequency transformer', *IEEE Trans. Power Electron.*, 1996, **11**, (1), pp. 33–42
- 31 Hurley, W.G., Wölfe, W.H., Breslin, J.G.: 'Optimized transformer design: inclusive of high-frequency effects', *IEEE Trans. Power Electron.*, 1998, **13**, (4), pp. 651–659
- 32 Bartoli, M., Noferi, N., Reatti, A., *et al.*: 'Modeling litz-wire winding losses in high-frequency power inductors', *IEEE Power Electron. Spec. Conf.*, 1996, **2**, pp. 1690–1696
- 33 Lavers, J.D., Bolborici, V.: 'Loss comparison in the design of high frequency inductors and transformers', *IEEE Trans. Magn.*, 1999, **35**, (5), pp. 3541–3543
- 34 Kondrath, N., Kazimierczuk, M.K.: 'Inductor winding loss owing to skin and proximity effects including harmonics in non-isolated pulse-width modulated dc-dc converters operating in continuous conduction mode', *IET Power Electron.*, 2010, **3**, (6), pp. 989–1000
- 35 Smeets, J.P.C., Krop, D.C.J., Jansen, J.W., *et al.*: 'Optimal design of a pot core rotating transformer'. Proc. IEEE Energy Conversion Congress and Exposition, September 2010, pp. 4390–4397
- 36 Howard, T.O., Carpenter, K.H.: 'A numerical study of the coupling coefficients for pot core transformers', *IEEE Trans. Magn.*, 1995, **31**, (3), pp. 2249–2253
- 37 Kazimierczuk, M.K., Sekiya, H.: 'Design of AC resonant inductors using area product method'. Proc. IEEE Energy Conversion Congress and Exposition, September 2009, pp. 994–1001
- 38 Cogirore, B., Keradec, J.P., Barbaroux, J.: 'The two-winding transformer: an experimental method to obtain a wide frequency range equivalent circuit', *IEEE Trans. Instrum. Meas.*, 1994, **43**, (2), pp. 364–371
- 39 Wojda, R.P., Kazimierczuk, M.K.: 'Winding resistance of litz-wire and multi-strand inductors', *IET Power Electron.*, 2012, **5**, (2), pp. 257–268
- 40 Wojda, R.P., Kazimierczuk, M.K.: 'Analytical winding size optimisation of solid-round-wire windings', *IEEE Trans. Ind. Electron.*, 2013, **60**, (3), pp. 1033–1041
- 41 Wojda, R.P., Kazimierczuk, M.K.: 'Analytical optimisation of solid-round-wire windings conducting dc and ac non-sinusoidal periodic currents', *IET Power Electron.*, 2013, **6**, (7), pp. 1462–1474
- 42 Magnetics, Inc.: 'Ferrite Cores', 2013